Pilz, M., Parolai, S., Petrovic, B., Silacheva, N., Abakanov, T., Orunbaev, S., Moldobekov, B. (2018): Basin-edge generated Rayleigh waves in the Almaty basin and corresponding consequences for ground motion amplification. - *Geophysical Journal International*, *213*, 1, pp. 301—316.

DOI: http://doi.org/10.1093/gji/ggx555

Geophysical Journal International

Geophys. J. Int. (2018) **213,** 301–316
Advance Access publication 2017 December 21
GJI Seismology

doi: 10.1093/gji/ggx555

Basin-edge generated Rayleigh waves in the Almaty basin and corresponding consequences for ground motion amplification

Marco Pilz,[1] Stefano Parolai,[2] Bojana Petrovic,[1] Natalya Silacheva,[3] Tanatkan Abakanov,[3] Sagynbek Orunbaev[4] and Bolot Moldobekov[4]

[1] *Helmholtz Center Potsdam – German Research Center for Geosciences, Helmholtzstr.* 7, 14467 *Potsdam, Germany. E-mail: pilz@gfz-potsdam.de*
[2] *National Institute of Oceanography and Applied Geophysics, Borgo Grotta Gigante* 42/*C,* 34010 *Sgonico, Italy*
[3] *Institute of Seismology of the Republic of Kazakhstan,* 75*A Al-Farabi Avenue,* 050060 *Almaty, Kazakhstan*
[4] *Central Asian Institute for Applied Geosciences, Timur Frunze St.* 73/2, 720027 *Bishkek, Kyrgyzstan*

Accepted 2017 December 20. Received 2017 December 12; in original form 2017 July 31

SUMMARY

During the past two centuries, several large earthquakes have caused extensive damages in the city of Almaty in Kazakhstan. Increasing the preparedness for future events, the definition of the optimal engineering designs for civil structures and the corresponding mitigation of earthquake risks involves the accomplishment of site response studies. To this regard, a temporary seismological network of 15 stations was installed in the city aiming at the accurate identification of local variations of site response at different locations. As the city is settled on a deep sediment-filled plain with laterally strongly varying thicknesses, bound to the south by the Tien-Shan mountain range, the city might face important site effects: large amplification and significant increase of shaking duration. In addition, surface waves in the low-frequency range around and slightly higher than the fundamental resonance frequency, which could be generated at the boundaries of the basin, can carry a large amount of energy. In turn, this will influence both the spatial distribution of the level of amplification and the temporal lengthening of ground motion significantly. For quantifying these effects, we apply complex trace analysis, which uses the instantaneous polarization characteristics of the seismic signal for separating waves arriving at a single site from different directions. In this way, secondary surface waves originating at various sites along the edge of the Almaty basin can be identified as well as their generation regions. After having assessed 1-D amplification effects with well-established techniques like the standard spectral ratio and the horizontal-to-vertical spectral ratio techniques, the results further indicate that thick layers of soft clay deposits and the 3-D structure of the basin give rise to lengthening of ground motion and high amplification values at low frequencies around 0.2 Hz. The steep structure of the sediment–bedrock interface at the southern edge of the Almaty basin can generate surface waves with distinct azimuths, meaning that the spatial variability of ground motion is not only related to a simple 1-D response but it can be strongly modified by secondary waves generated at the margin of the basin.

Key words: Asia; Site effects; Surface waves and free oscillations; Wave propagation.

1 INTRODUCTION

Central Asia, being located in the collision zone between the Eurasian and Indo-Australian lithosphere plates, is one of the seismically most active regions in the world. Over the centuries, the region, although not very densely populated in former times, has been affected by strong earthquakes repeatedly. Already before the actual founding of Verny (renamed to Alma-Ata in 1921 and to Almaty in 1993) as a Russian fort in 1854, large earthquakes are known to have taken place in the area. Examples are given by the 1475 event in the vicinity of Burana in today's Kyrgyzstan (Mushketov & Orlov 1893; see Fig. 1) and in 1770 more western near Belovodskoe (Mushketov & Survorin 1891; Mushketov 1899; Chedia *et al*. 1998). Although the given catalogues provide a purely descriptive approach, the epicentral macroseismic intensities (Medwedew-Sponheuer-Kárník MSK-64 scale) were estimated as I = IX for the 1475 event and I = VIII for the 1770 event (Korjenkov *et al*. 2004). In 1865, an M 6.4 earthquake ruptured near Merke (Ulomov *et al*. 2002) and on 1885 August 2 another one near Belovodskoe in the Chu depression (M 6.7 to 6.9, Ignatiev 1886; Bindi *et al*. 2014).

The following years are marked by a cluster of strong events: On 1887 June 9, the Verny earthquake (M 7.3, I = IX–X) with

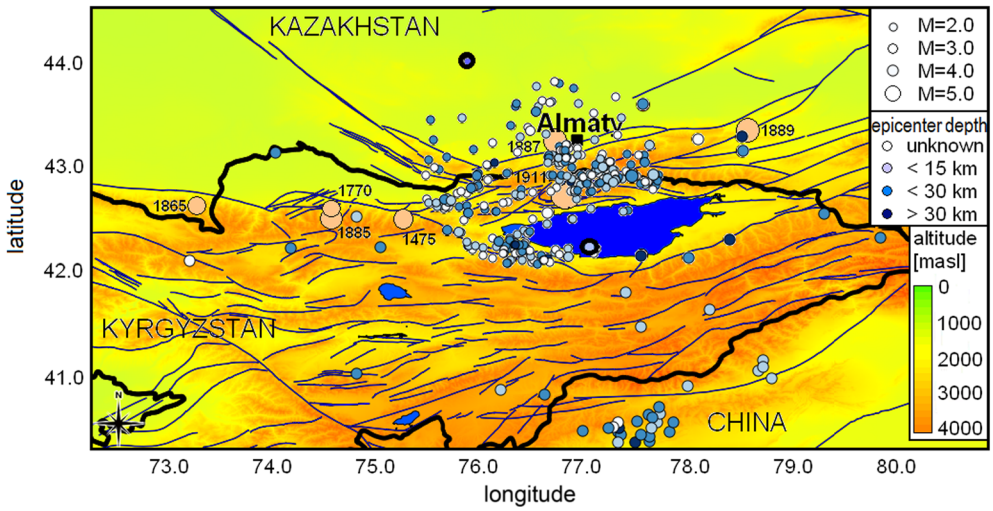

Figure 1. Location of the city of Almaty. The epicentres of the local and regional earthquakes used in this study (blue dots, colour-coded for depth) and the main active faults (thin lines, Trifonov *et al*. 2002) are indicated. The bold-framed dots indicate the analysed M 4.3 events of 2014 June 13 at a distance of 120 km south of Almaty and of 2014 July 30 northwest of Almaty. For strong historical earthquakes mentioned in the text, the light red dots indicate the hypocentre location and the year of occurrence.

the epicentre near modern Almaty caused severe damages in the city occupied by around 23 000 inhabitants at that time (Mushketov 1888; Vershinin 1889). On 1889 July 12, the Chilik earthquake (M 8.3) with its epicentre located 120 km east of modern Almaty at the eastern end of Trans-Ili Alatau range caused a level of macroseismic intensity of VII–VIII on the MSK-64 scale in Verny/Almaty (Korjenkov *et al*. 2004). The Kemin earthquake (also called Chon-Kemin event) of 1911 January 4 (M 7.8) was located to the south of modern Almaty although the distribution of intensity data points is not able to define a unique solution for the event location (Bindi *et al*. 2014). Within the first 10 km the event might have reached an intensity of I = X–XI (Bogdanovich 1911; Velitzky 1911; Bogdanovich *et al*. 1914). Even in Almaty severe destruction has been observed as almost every house has been damaged (Nurmagambetov 1999; Nurmagambetov *et al*. 1999; Abdrakhmatov *et al*. 2002). The Agency for Emergencies of the Republic of Kazakhstan estimates that for a similar event nowadays the total number of people injured or affected would be in the order of 300 000. Of these, some 75 000 people would likely be killed (Rau 2003 and references therein). Approximately one third of all residential buildings in Almaty would be destroyed. To complicate matters further, the city is endangered by several faults which have not been associated with any previous event but might have the potential to generate a large event (SNIP 2001). Most of these faults were inspected comprehensively during Soviet times in the 1960s and 1970s but nowadays most reports are not accessible anymore.

For assessing the regional level of seismic hazard, early seismic zoning maps for the whole Union of Soviet Socialist Republics (USSR) were released in 1957, 1968 and 1978 accompanied by detailed seismic zoning (DSZ) and seismic microzoning studies for the largest cities of the USSR taking into account local seismotectonic, seismic, ground and further natural conditions based on engineering-geological and geophysical studies (an overview is given in McGuire 2004). After the collapse of the Soviet Union in 1991, the level of seismic hazard was re-evaluated, mainly following a probabilistic approach. For Almaty, DSZ maps were released in terms of both intensity and peak ground acceleration (Kyurskeyev *et al*. 1993) and probabilistic hazard studies have been carried out (Mikhailova 1996).

These latter studies pointed out that, due to its location near the northern flanks of the Alatau range on thick layers of friable deposits of the Almaty depression, the underlying sedimentary cover will have a strong influence on the level and the duration of shaking and the corresponding level of hazard. A common explanation for the modification of ground motion is the trapping of seismic energy due to the impedance contrast between the layered sediments and the underlying bedrock. In case of horizontal layering of the sediments and when the local *S* wave soil profile is known, the site amplification can be routinely evaluated in the frequency domain using the 1-D transfer function. However, if the site conditions cannot be described by simple 1-D layering as in the case of Almaty (Silacheva *et al*. 2014a), simple analytic tools can hardly provide a proper quantification of the level of amplification.

When lateral heterogeneities are present, additional phenomena like focusing and/or scattering of seismic waves and the appearance of locally generated surface waves come into play. Theoretical evidences of such basin-induced surface waves have been demonstrated by many researchers already decades ago (e.g. Aki & Larner 1970; Boore *et al*. 1971; Trifunac 1971; Hong & Helmberger 1978; Bard & Bouchon 1980a, 1980b; Horike *et al*. 1990; Narayan 2005; Hallier *et al*. 2008, 2012). Such waves, which propagate horizontally across the basin even in the case of body wave incidence, are mainly generated at the basin edge. They are caused by the complex interaction of incident body waves and diffracted waves. Although the basin edge geometry was found to have a more significant influence on the level of amplification and the lengthening of ground motion than the soil layering itself (Semblat *et al*. 2005), strong lateral heterogeneities of the sedimentary cover can further modify the direction and properties of the surface waves within the basin (e.g. Koketsu & Kikuchi 2000; Furumura & Hayakawa 2007; Huang *et al*. 2010; Roten *et al*. 2011; Takemura *et al*. 2015). Observational evidence was first reported by Hanks (1975) with reference to the 1971 San Fernando earthquake and by Toriumi (1975) for the Osaka basin. Later, Liu & Heaton (1984) and Vidale & Helmberger (1988) confirmed the interpretation of low-frequency strong motions for the San Fernando and Los Angeles Basins. The destructive Michoacan, Mexico earthquake of 1985 provided further evidence of the important role of basin-induced surface waves

(e.g. Anderson *et al*. 1986; Kawase 1987). The 1994 Northridge, California (M_w 6.7, Davis *et al*. 2000) and the 1995 Hyogo-ken Nanbu earthquake in Japan (M_w 6.9, Kawase 1996) are further impressive examples where these effects have played a major role in the spatial distribution and the amount of damage. While generally both Rayleigh and Love waves are induced at the basin edge, their relative contribution has been found to depend on the actual basin properties (e.g. Rovelli *et al*. 2001, Cornou *et al*. 2003; Yoshimoto & Takemura 2014). As a consequence, a proper understanding of wave propagation and the corresponding processes leading to wave diffraction and scattering inside sedimentary basins is of major seismological and engineering interest.

Waveform recordings at sedimentary basin sites, however, pose another challenge as they are often characterized by a complex superposition of various arrivals hardly allowing a direct identification of any secondary waves. Separating different wave types arriving at different times based on their instantaneous polarization attributes, Rene *et al*. (1986) and Vidale (1986) proposed a complex polarization analysis for the identification of Rayleigh wave phases. The main disadvantage of this method is that no information on the temporal variation of the frequency content can be obtained, meaning that the frequency range of interest has to be chosen in advance. Moreover, since only the vertical and radial components of ground motion are analysed, the method relies on a fixed direction of wave propagation. While this assumption might be true for active seismic studies, it might have limited validity when basin-edge generated surface waves are analysed.

An extension of this analysis to the time–frequency (*t–f*) domain, however, can allow separating different seismic phases even when multiple waves arrive at the same time at a single site. Pinnegar (2006) introduced a *t–f* polarization analysis based on the *S* transform (Stockwell *et al*. 1996) that produces *t–f* spectra of the polarization characteristics of three-component seismic signals. Using these spectra, the signal can be separated into linear and circularly polarized components, making it suitable for identifying Rayleigh waves. By applying *t–f* domain filters based on the *S* transform, Meza-Fajardo *et al*. (2015) introduced a method to extract Rayleigh and Love waves arrivals of a seismogram. While for the mentioned applications the direction of wave propagation does not have to be known in advance, they rely on the assumption that Love waves and Rayleigh waves share the same backazimuth from the source to the analysed site. However, when analysing the wavefield in a sedimentary basin, one is dealing with a superposition of various scattered waves. The waves can be generated at different locations with the possibility to reach a single station at the same time but from different directions. For example, Gao *et al*. (1996) analysed seismograms of aftershocks of the Northridge earthquake and demonstrated that the amplification pattern in the Santa Monica zone did change for different hypocentre positions. This means that such requirement for basin-edge induced surface waves generated along the direct path between the hypocentre and the site of interest has to be relaxed. Each phase in the seismogram has to be separated independently from the arrival direction and time.

In this study, we analyse earthquake recordings for identifying spatial variability of ground motion based on standard site response methods, namely the horizontal-to-vertical spectral ratio (HVSR) from earthquake recordings and the standard spectral ratio technique. We consider site-specific amplification accounting not only for the modulus, but also for phase modifications related to local site conditions, by making use of the mean group delay algorithm proposed by Papoulis (1962) and Sawada (1998). We further analyse polarization attributes for identifying basin-edge generated Rayleigh waves and their direction of propagation (Petrovic *et al*. 2018). This method is based on a single station analysis, meaning that extended seismic arrays, as commonly used (e.g. Frankel *et al*. 1991; Cornou *et al*. 2003), are not required. When applied to a network of seismic stations in a basin, the method further allows locating the source of the diffracted waves. We test the performance of the technique using a real-world data set collected in the Almaty basin.

2 NETWORK INSTALLATION AND EARTHQUAKE DATA

Research activities on earthquakes in Kazakhstan were increased significantly in the 1970 s during the installation of Soviet strong motion network. An analogue local network at eight sites located in different engineering-geological conditions in the central districts of Almaty has been installed in the early 1980s. It was replaced in 2000 by 15 digital strong motion stations (Silacheva *et al*. 2014b). The existing network has been complemented by 15 weak motion instruments (Guralp CMG-3ESP broad band sensors with an eigenperiod of 120 s) between March and November 2014, partially co-located but also extending the network coverage in the outskirts of the city on different geological materials. All stations were installed inside buildings (on the ground floor or, if possible, in cellars), and were placed in their room's corner. The stations were synchronized using GPS reference time and the signal was recorded at each site with a sampling rate of 100 samples per second. Precise geological information (Kulikovsky 1973), however, is available only for the central part of the city, which is characterized by sedimentary layers of different age with some isolated spots of fluvial deposits, see Fig. 2. The sedimentary cover reaches a thickness of more than 3 km for the central part of the study area. To the southeast of the city, the bedrock composed of Palaeozoic granites is outcropping.

From the continuous data streams recorded by the network, the recordings of 121 earthquakes were extracted using the bulletin of the SEME MES RK (Seismological Experimental and Methodical Expedition of the Committee of Science of the Ministry of Education and Science of the Republic of Kazakhstan) and a slightly modified version of the procedure proposed by Galiano-Merino *et al*. (2008). The list includes earthquakes with magnitudes between M_L 2.0 and M_w 5.6 that occurred in a depth range between 8 and 40 km and at distances between about 10 and 523 km from the central station Al04. Most events occurred to the south of the city along the northern Tien-Shan between Kazakhstan and Kyrgyzstan. The distribution of their epicentres and depths is shown in Fig. 1. For the respective time period, we further included 22 teleseismic events with magnitudes between M_w 7.0 and M_w 8.1.

3 HORIZONTAL-TO-VERTICAL SPECTRAL RATIOS

Several techniques have been utilized to evaluate site response. Among the so-called non-reference site methods (Bard 1995), the HVSR method (Lermo & Chavez-Garcia 1993) is commonly used. The method allows source and path contributions to be removed from the recordings by means of a deconvolution procedure assuming that the vertical component of the ground motion is free of near-surface influence. Thus, the site effect can be evaluated by a division of the amplitude spectrum of the horizontal component with the spectrum of the vertical component of the same event.

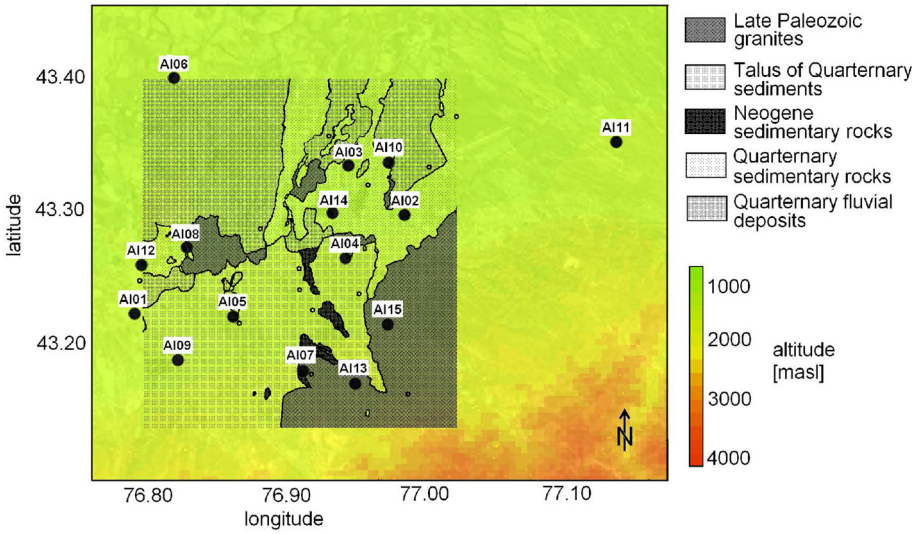

Figure 2. Locations of temporary network sites (black dots) installed in the city of Almaty. The small circles represent the stations of the permanent Kazakh strong motion network. Geological information for the central part is taken from Kulikovsky (1973).

From the continuous recordings, we only selected the most energetic *S* wave window starting 3 s before its arrival until the *S* wave energy reaches 90 per cent of its total energy (Examples of recordings and analysed time windows are shown in top three rows of Figs 6 and 7). After correcting for instrumental response, each window was cosine tapered (5 per cent) and a fast Fourier transformation for each seismometer component was performed. Spectral amplitudes were smoothed using the Konno & Ohmachi (1998) recording window ($b = 40$), ensuring smoothing of numerical instabilities while preserving the major features of the earthquake spectra that were considered valid only when the signal-to-noise ratio (SNR) is greater than 3.

Representative results of six stations installed in different parts of the city are shown in Fig. 3. The HVSR for all stations show a broad but only moderate amplification at frequencies between 1 and 10 Hz with amplitude maxima around 3. Whereas for stations Al01 and Al05 installed in the central part of the city an amplitude decrease for frequencies smaller than ∼3 Hz is found, such amplitude decrease is slightly shifted towards lower frequencies for stations in the northern part of the city. Al06 and Al10, for which the thickness of the lower Quaternary deposits and fine-grained sediments exceeds 500 m, are characterized by an amplitude decrease only for frequencies smaller than 1 to 2 Hz. In the southern part of the city, the thickness of the shallow sedimentary rocks of the Neogene period reaches a maximum of 300 m. These rocks do not reach the surface and are further covered by sandy and loamy tali of the Quaternary period. In the foothills zone at the southern and eastern edges of the city, the existence of dense pebble layers on top of the Palaeozoic rocks in line with shallow impedance contrasts might be the cause of several narrow peaks with moderate amplitudes around 2 in the earthquake HVSR (e.g. Al15). For some sites (e.g. Al01, Al06 and Al10), the existence of a low-amplitude peak at frequencies around 0.15–0.25 Hz might indicate the existence of a deep but rather small impedance contrast between the sedimentary cover and the Palaeozoic bedrock.

4 STANDARD SPECTRAL RATIOS

The standard spectral ratio (SSR) technique (Borcherdt 1970) is based upon comparing records at nearby sites, using one as the reference. The method relies on the assumption that recordings at the reference site (in general, a station installed on outcropping hard bedrock) contain the same source and path effects as records from the other sites. This is generally warranted for epicentral distances larger than about five times the station distance (Duval 1996; Bard 1999). Therefore, differences observed with respect to the reference site are mainly due to local site effects, meaning that the spectral ratio can directly provide the site response.

As this approach is based on the ratio of the modulus of the Fourier spectra, it only allows the frequency-dependent amplitude modification of shaking to be retained, while it does not grant a comparison of the phase characteristics of records. When several earthquakes are analysed and their results are averaged, the ratio of the complex Fourier spectra will tend to remove 2-D and 3-D effects due to the different arrival times of the seismic waves at the investigated site and the reference site. Nonetheless, an extension of the classical spectral ratio method, the mean group delay technique proposed by Papoulis (1962) and Sawada (1998), can allow the phase modifications to be obtained in a robust way.

For estimating the complex site response, a two-step approach is followed. In a first step, the amplitude is estimated by the classical standard spectral ratio method, while in a second step the phase component of the spectrum is obtained based on the mean group delay technique. The latter basically allows for each frequency to measure the arrival time of each phase in the seismogram by differentiating the (unwrapped) phase spectrum, $\Phi(\omega)$, obtained by Fourier transforming the signal, with respect to the angular frequency ω. The obtained quantity $T_{\mathrm{gr}} = \frac{\partial \Phi(\omega)}{\partial \omega}$, which has a time dimension, is defined as the group delay time. This variable, however, is affected by strong scatter, meaning that a regularization operator has to be applied. This operation accounts for the amplitude spectrum of the signal and considers a smoothing function in the frequency domain. In turn, the measured group delay depends slightly on the nature and amplitude of the signal but, more significantly, on its SNR. Further details can be found, for example, in Beauval *et al*. (2003) and Pilz & Parolai (2016).

Station Al13, although located on Palaeozoic granites (see Fig. 2), was found not to be an ideal reference site due to moderate amplification for $f > 1$ Hz (see Fig. 3). The station, however, might still serve as a reference station for the low-frequency range. In fact, for

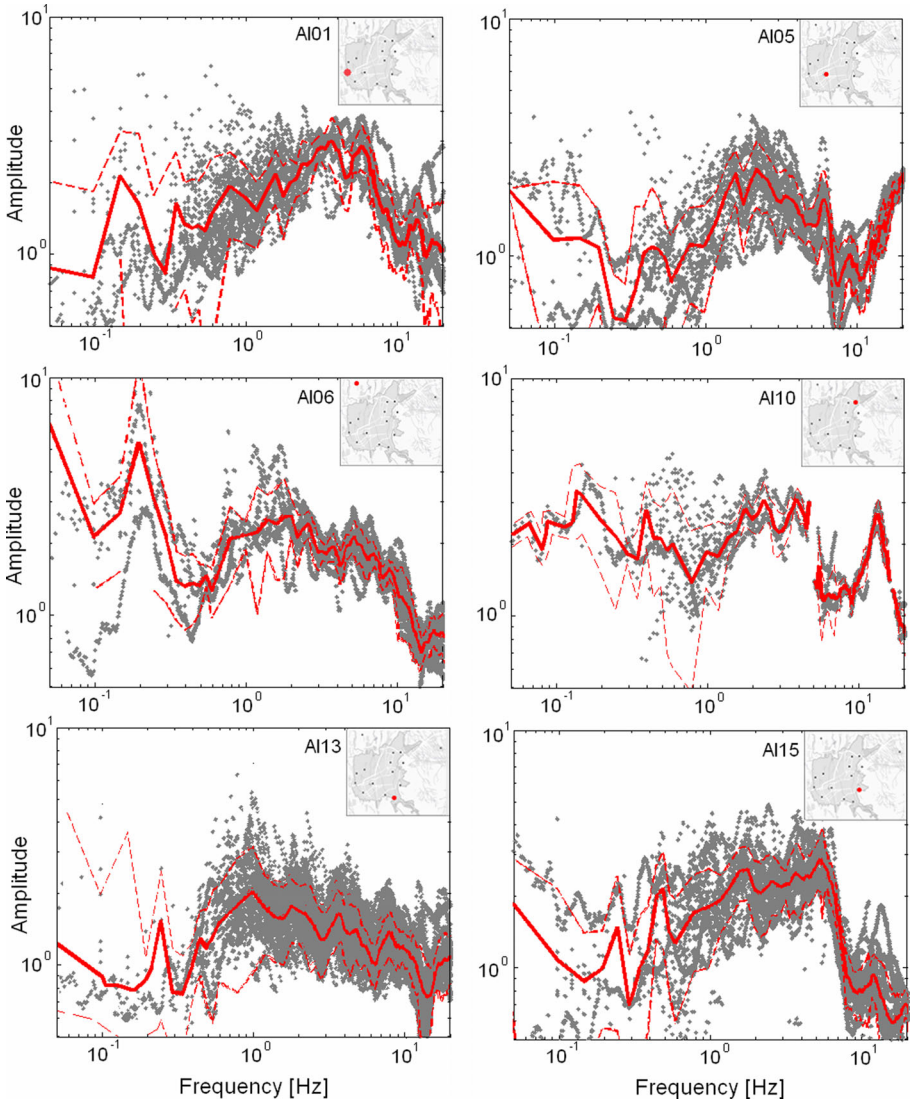

Figure 3. Earthquake horizontal-to-vertical spectral ratios for six seismic stations installed in Almaty. The grey dots correspond to frequencies for which the signal-to-noise ratio is larger than 3. The red lines represent the mean plus/minus one standard deviation. In the inset map, the red dot indicates the location of the station presented and the dark-grey colour represents the populated areas of Almaty.

$f < 1$ Hz, the HVSR are not amplified significantly. Additionally, only minor propagation effects are affecting the SSR results over this frequency range due to the close distance between Al13 and the other stations of the network.

The results in Fig. 4 show that the SSRs for all stations are characterized by a rather similar behaviour with a broad amplification in the low-frequency range. While for Al01 and Al06 a moderate amplification maximum around 0.2 Hz is found, for Al05, Al10 and Al15 there is even an amplitude increase towards lower frequencies. At frequencies around and below 1 Hz, low amplitudes with values being only slightly larger than 1 are found. For frequencies higher than 1 Hz, the amplitudes of the SSRs and earthquake HVSRs lie in the same range due to the amplification at the reference site. Although in the high-frequency range ($f \approx 10$ Hz) the earthquake HVSR at the reference site is characterized by values around 1, its trough around 12 Hz causes a narrow amplification peak in the SSR at several other network sites.

Fig. 5 shows an example of the group delay spectrum due to site effects, that is, the frequency- dependent lengthening of signal duration between the soft soil site and the reference site. When applying the group-delay method, the modulus of the site response function, that is, the HVSRs and SSRs remain unchanged. The frequencies, however, at which maxima of duration lengthening occur (in general frequencies around 0.2–0.4 Hz show a moderate lengthening of duration in the order of 3–5 s, red lines in Fig. 5), do not correspond to the frequencies of the maximum SSRs. These frequencies are slightly higher than the fundamental resonance frequency of the site being around 0.15–0.25 Hz (Fig. 3). Similar qualitative observations have already been made for the Kanto basin in Japan (Yoshimoto & Takemura 2014) and the Mygdonian Basin in Greece (Maufroy *et al*. 2017). Analogously, we see that the two indicators of site effects are not correlated directly, meaning that the maximum duration lengthening is not related to resonance of body waves but rather to the excitation of local surface waves (e.g. Cornou *et al*. 2003). For frequencies much higher than the fundamental resonance frequency of the site, this effect becomes less obvious. For $f > 10$ Hz, the group delay time is characterized by rather small values around 1, meaning that the phase changes are no longer significant, even though some amplification effects might still exist.

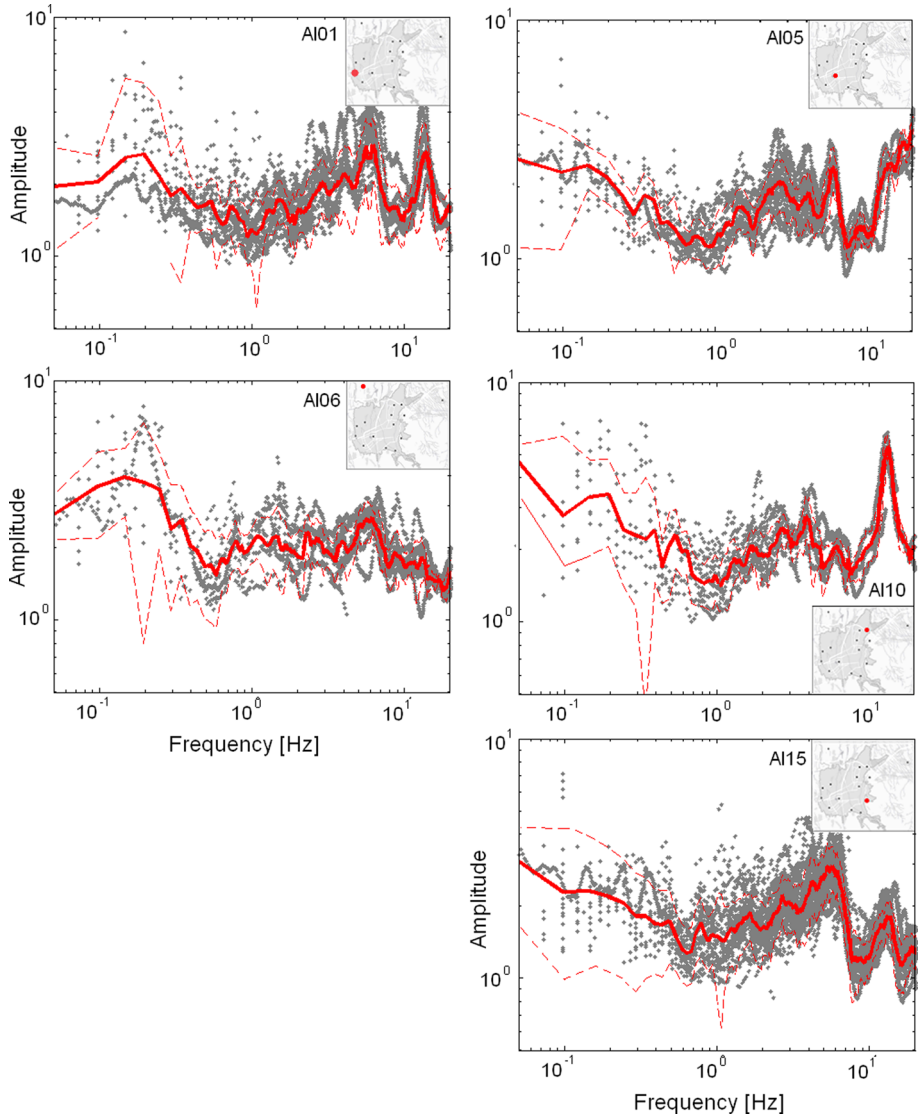

Figure 4. Standard spectral ratios (grey dots) computed at five representative stations against the corresponding spectrum at reference station Al13 for signal-to-noise ratios larger than 3. The red lines represent the mean plus/minus one standard deviation. In the inset map, the red dot indicates the location of the station presented and the dark-grey colour represents the populated areas of Almaty.

A remarkable difference in terms duration lengthening can be found between events occurring north of Almaty (black dots in Fig. 5) and southern sources, which represent the majority of recorded events (grey dots in Fig. 5). Although events from the north do not generate large group delay times and duration lengthening, for southern sources, a clear extension of ground motion is found. This might be due to the asymmetric shape of the Almaty basin which is bordered to the south by the northern fringe of the Tien-Shan mountain range, whereas to the north, the Almaty basin turns into the Ili basin which slowly merges into the deserts and steppes.

5 POLARIZATION ANALYSIS

For identifying the kind of waves responsible for the presented amplification patterns, we estimate the waves' polarization attributes based on the procedure of Petrovic *et al.* (2018). After integrating the recorded velocities to displacement time histories (following Boore & Bommer 2005), we first try to identify possible basin-edge generated surface waves at network sites. Based thereon, we determine possible generation regions of the surface waves along the basin edge.

As earthquake recordings, especially those from urban areas, are often affected by noise which might degrade the quality of seismic records, an *ad hoc* denoising procedure is first carried out. This method is based on the calculation of the *S* transform of the recorded signal (Parolai 2009) which allows a decomposition of the signal in the *t–f* domain by combining the short-time Fourier transform (Gabor 1946) and the continuous wavelet transform (Morozov & Smithson 1996) with a moving and scalable localizing Gaussian window.

Stockwell *et al.* (1996) provided a formal expression of the *S* transform of a function $h(t)$

$$S(\tau, f) = \int_{-\infty}^{\infty} h(t) \left[\frac{|f|}{\sqrt{2\pi}} \exp\left(\frac{-f^2(\tau - t)^2}{2} \right) \exp(-2\pi i f t) \right] \mathrm{d}t. \quad (1)$$

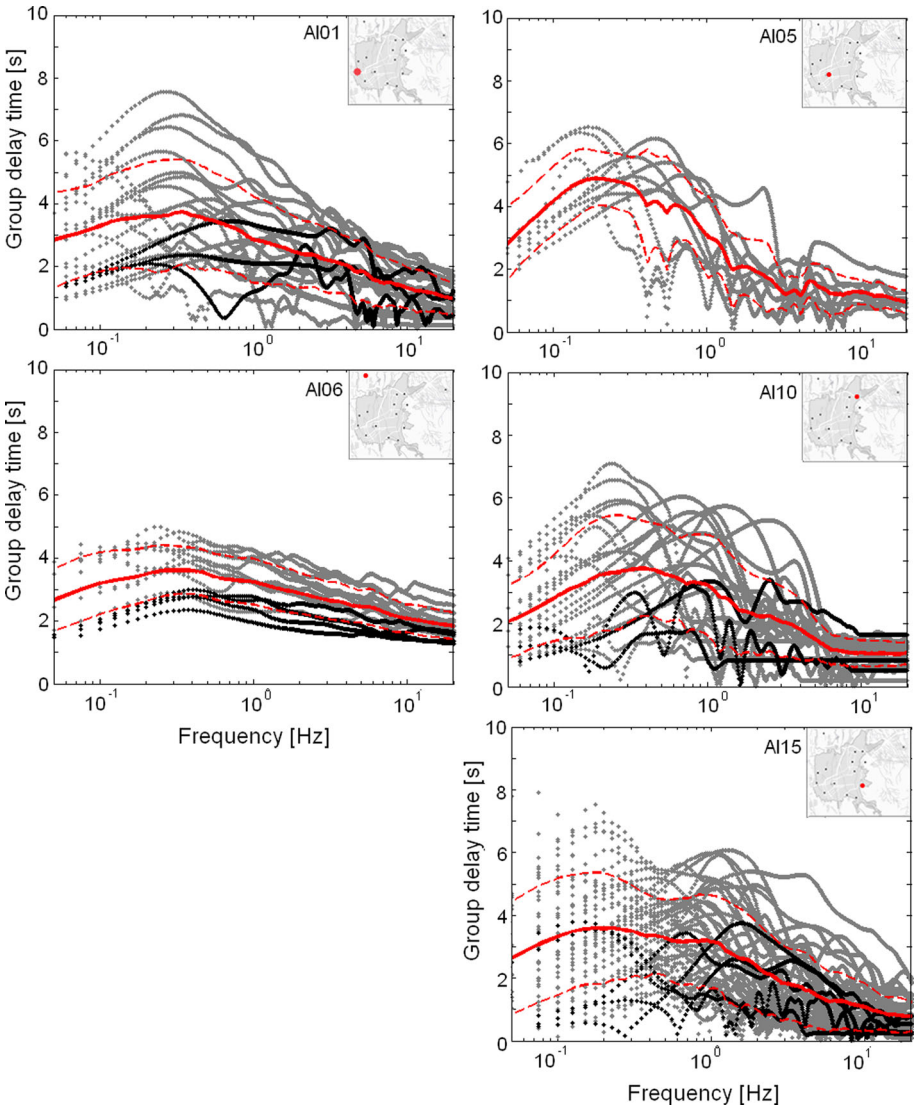

Figure 5. Mean group delay time (grey dots) with respect to the corresponding reference station Al13 for events with an SNR > 3. The black dots represent earthquakes from the northern azimuthal sectors. The red lines indicate the mean plus/minus one standard deviation. In the inset map, the red dot indicates the location of the station presented and the dark-grey colour represents the populated areas of Almaty.

Herein, t represents time, f is frequency, and τ is a parameter controlling the position of the Gaussian window along the time axis. After denoising of the seismogram, the filtered results are transformed back in the time domain. Such S transform decomposition already allows identifying and isolating dispersive wave trains (e.g. Parolai 2009).

For estimating the direction of wave propagation, the maximum amplitude for every point in the t–f plain of the S transform of the horizontal components is identified by rotating the coordinate system in a finite, but large, number of steps $\Delta\theta$ in the horizontal plane between 0 (north) and π (south) until one of the horizontal coordinate axes points in the direction of the maximum ground motion amplitude. Correspondingly, the maximum value (from now on referred to as the denoised S transform of the optimized horizontal component) as well as the direction of the maximum amplitude (as θ and $\theta + \pi$ due to azimuthal ambiguity) are obtained for every point in the t–f space. As we do not assume sharp lateral velocity contrasts which might cause significant deviations of the wave trains, this direction is assumed to correspond to the direction towards the basin edge where secondary Rayleigh waves are generated.

As for real-world recordings Rayleigh waves might deviate from their standard prograde or retrograde particle motion (Alterman & Karal 1968; Stephenson 2003; Tanimoto & Rivera 2005), we identify the polarization attributes of the high-energetic arrivals in the t–f plain. In a first step, for isolating spots of high energy in the t–f plain, we apply a threshold of 20 per cent of the maximum energy of the denoised S transform on both the vertical and the optimized horizontal components. Based on numerical simulations, Petrovic *et al*. (2018) have shown the appropriateness of this threshold.

In turn, for every point in the t–f plain, we calculate the multi-component instantaneous amplitude $A_i(\tau, f)$

$$A_i(\tau, f) = \sqrt{(\mathrm{Re}[S_i(\tau, f)])^2 + (\mathrm{Im}[S_i(\tau, f)])^2} \quad (2)$$

with $i = v$ for the vertical and $i = h$ for the optimized horizontal component.

The instantaneous phase difference $\varphi(\tau, f)$ is calculated

$$\varphi(\tau, f) = \tan^{-1}\left[\frac{\mathrm{Re}\,[S_h(\tau, f)]\,\mathrm{Im}\,[S_v(\tau, f)] - \mathrm{Re}\,[S_v(\tau, f)]\,\mathrm{Im}\,[S_h(\tau, f)]}{\mathrm{Re}\,[S_v(\tau, f)]\,\mathrm{Re}\,[S_h(\tau, f)] + \mathrm{Im}\,[S_v(\tau, f)]\,\mathrm{Im}\,[S_h(\tau, f)]}\right] \quad (3)$$

where Re $[S(\tau, f)]$ and Im $[S(\tau, f)]$ represent the real and imaginary part of the S transform and S_v and S_h refer to the vertical and optimized horizontal component. The phrase 'instantaneous' indicates the functional dependence on time.

For the calculation of the polarization attributes, the Cartesian representation of the instantaneous amplitude and the instantaneous phase difference along the horizontal axes is rotated into the ellipse representation using the rules of geometric algebra. This representation is based on the semi-major and semi-minor axes $a(\tau, f)$ and $b(\tau, f)$ of the polarization ellipse,

$$a(\tau, f) = \sqrt{\frac{S_0(\tau, f) + \sqrt{S_1^2(\tau, f) + S_2^2(\tau, f)}}{2}} \quad (4a)$$

$$b(\tau, f) = \sqrt{\frac{S_0(\tau, f) - \sqrt{S_1^2(\tau, f) + S_2^2(\tau, f)}}{2}}\,. \quad (4b)$$

The three Stokes parameters S_0, S_1 and S_2 in eqs (4a) and (4b) are defined as the measurable quantities completely determining the polarization state of the wave. They can be written as

$$S_0(\tau, f) = A_v^2(\tau, f) + A_h^2(\tau, f) \quad (5a)$$

$$S_1(\tau, f) = A_v^2(\tau, f) - A_h^2(\tau, f) \quad (5b)$$

$$S_2(\tau, f) = 2A_v(\tau, f)\,A_h(\tau, f)\cos[\varphi(\tau, f)] \quad (5c)$$

where A_v and A_h represent vertical and horizontal instantaneous amplitudes, respectively, (eq. 2).

In the t–f domain, the instantaneous reciprocal ellipticity $\rho(\tau, f)$ is defined as the ratio of the semi-minor to the semi-major axis,

$$\rho(\tau, f) = \frac{b(\tau, f)}{a(\tau, f)}\,. \quad (6)$$

For further analyses, we exclude waves that are either polarized linearly ($\rho(\tau, f) = 0$) or circularly ($\rho(\tau, f) = 1$) and we will refer to the signed instantaneous reciprocal ellipticity (from now on called polarization σ, Smith & Ward 1974), that is,

$$\sigma(\tau, f) = \mathrm{sgn}\,[\varphi(\tau, f)]\,\rho(\tau, f)\,. \quad (7)$$

$\sigma(\tau, f)$ is negative or positive according to whether particle motion is prograde or retrograde.

In order to assign a specific geomorphical feature at the basin edge being able to generate secondary waves, only sufficiently spatially resolved information on the shape of the basin edge is required. These regions can be determined from a single station by a line striking with $\theta \pm \Delta\theta$ and crossing the edge of the basin. $\Delta\theta$ corresponds to the rotation step defined above. These intersection points are not related to the original station-to-hypocentre backazimuth.

6 POLARIZATION RESULTS

The results in terms of t–f analysis, σ and θ for a representative regional M 4.3 event, which occurred on 2014 June 13 at a distance of around 120 km south of Almaty at a depth of 12 km, and an event of similar magnitude and distance, which occurred on 2014 July 30 northwest of the city at a depth of 18 km, (bold-lined dots in Fig. 1) are compared in Figs 6 and 7 for three representative network sites on different geological materials. Although for both events the body wave arrivals can clearly be identified (reddish colours in Figs 6 and 7), even a close look at the displacement time-series seismograms hardly allows distinguishing secondary low-frequency waves univocally as the shapes of the waveforms appear to be rather complex. Such complex behaviour is likely due to the conversion and superposition of different types of waves having different frequencies and propagation directions, in turn arriving at one site at the same or similar time. The denoised S transforms of the recorded waveforms clearly indicate some high energy spots in the t–f plain in the low frequency band between 0.15 and 0.4 Hz for the event south of Almaty (Fig. 6, black ellipses in fourth and fifth row from top). As can be seen in the t–f analysis, the noise contribution (bluish colours) is not significant and the dispersive wave trains (high-energy low-frequency arrivals around 0.15–0.25 Hz gradually followed by higher frequency arrivals) are imaged more clearly. Remarkably, the frequency band of these high energy values corresponds to the same frequency range between 0.15 and 0.4 Hz for which a lengthening of ground motion of several seconds is found at all network sites (grey dots in Fig. 5).

On the contrary, for none of the analysed events with epicentres north of the city distinct low-frequency arrivals with sufficient SNR have been found. Exemplarily, Fig. 7 shows that while body wave arrivals can clearly be identified, no low-frequency waves can be observed after the S wave arrival. As the goal of the manuscript lies on the characterization of secondary surface waves, no calculation of the polarization properties is carried out for the 2014 July 30 event and we will focus on the event of 2014 June 13 in the following.

Although for this event the attributes of the signed reciprocal ellipticity and the direction of propagation for each of the energy maxima of the S transform on the vertical and the optimized horizontal components (black ellipses in second row from bottom and bottom row in Fig. 6 corresponding to the ellipses indicating high-energy spots of the S transform) do show some variation at first glance, clear preferential values for both parameters are found. To this regard, we calculate the weighted mean of the values inside the ellipses. For Al01, Al05 and Al12, the signed reciprocal ellipticity is centred around zero (Fig. 8 top). Further network sites indicate a slight tendency towards positive values, that is, retrograde particle motion. This is expected for Rayleigh waves. Moreover, a preferential direction of propagation around π is found for network sites in the western part of the city (e.g. Al01, Al06, Al08) whereas for eastern stations (e.g. Al03, Al04, Al10), the values of θ are centred around $\pi/4$ (Fig. 8 bottom). This means that the low-frequency signal reaches most network sites from different directions. The lines striking with an angle corresponding to the direction of propagation coincide in the same region along the basin edge (Fig. 9). Remarkably, almost none of the generation sites along the basin edge resembles the direction of the hypocentre (white arrow in Fig. 9).

Although strong lateral heterogeneities of the sedimentary cover might cause deviations of propagation when surface waves travel across the basin (e.g. Furumura & Hayakawa 2007; Roten *et al.* 2011), the influence of such directivity patterns is expected to be of minor influence and within the parameters' uncertainty for the Almaty basin. Based on the analysis of 542 exploration wells spread over the entire city, the Japan International Cooperation Agency (2009) has documented sharp velocity contrasts only for the uppermost few tens of meters between sites in the southern and northern

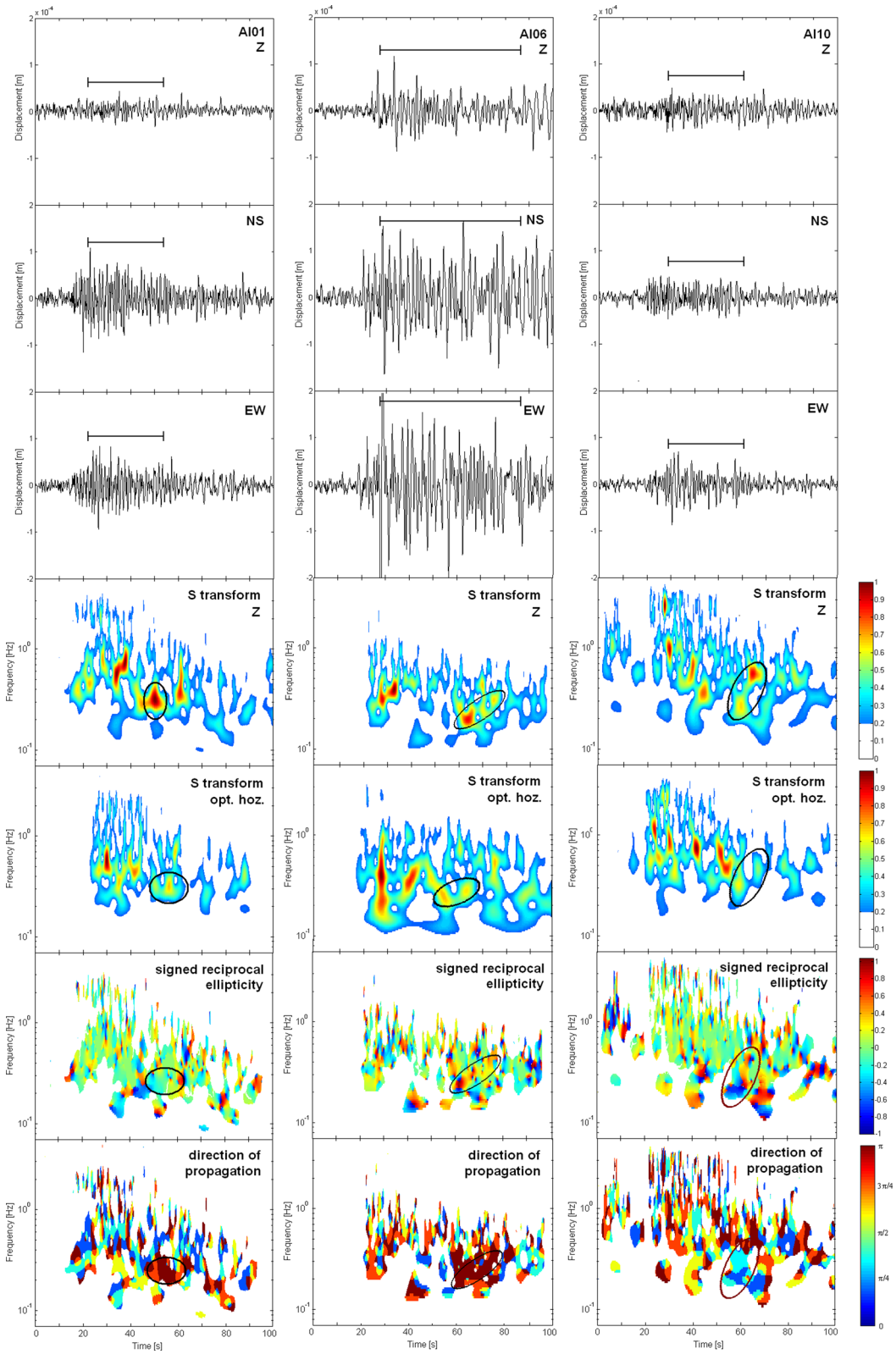

Figure 6. The displacement time-series for the vertical (top row), NS (second row from top) and EW components (third row from top), normalized time–frequency analysis (*S* transform) of the vertical (fourth row from top) and of the optimized horizontal component (fifth row from top), signed reciprocal ellipticity σ (second row from bottom) and direction of propagation θ from south (bottom row) for the 2014 June 13 event south of Almaty for stations Al01 (left), Al06 (middle) and Al10 (right). A threshold of 20 per cent of the maximum energy of the denoised *S* transform is applied both to the vertical and the optimized horizontal components. Selected areas of high energy are indicated by a black ellipse. The time windows for *S* wave analyses (HVSR and SSR) are indicated.

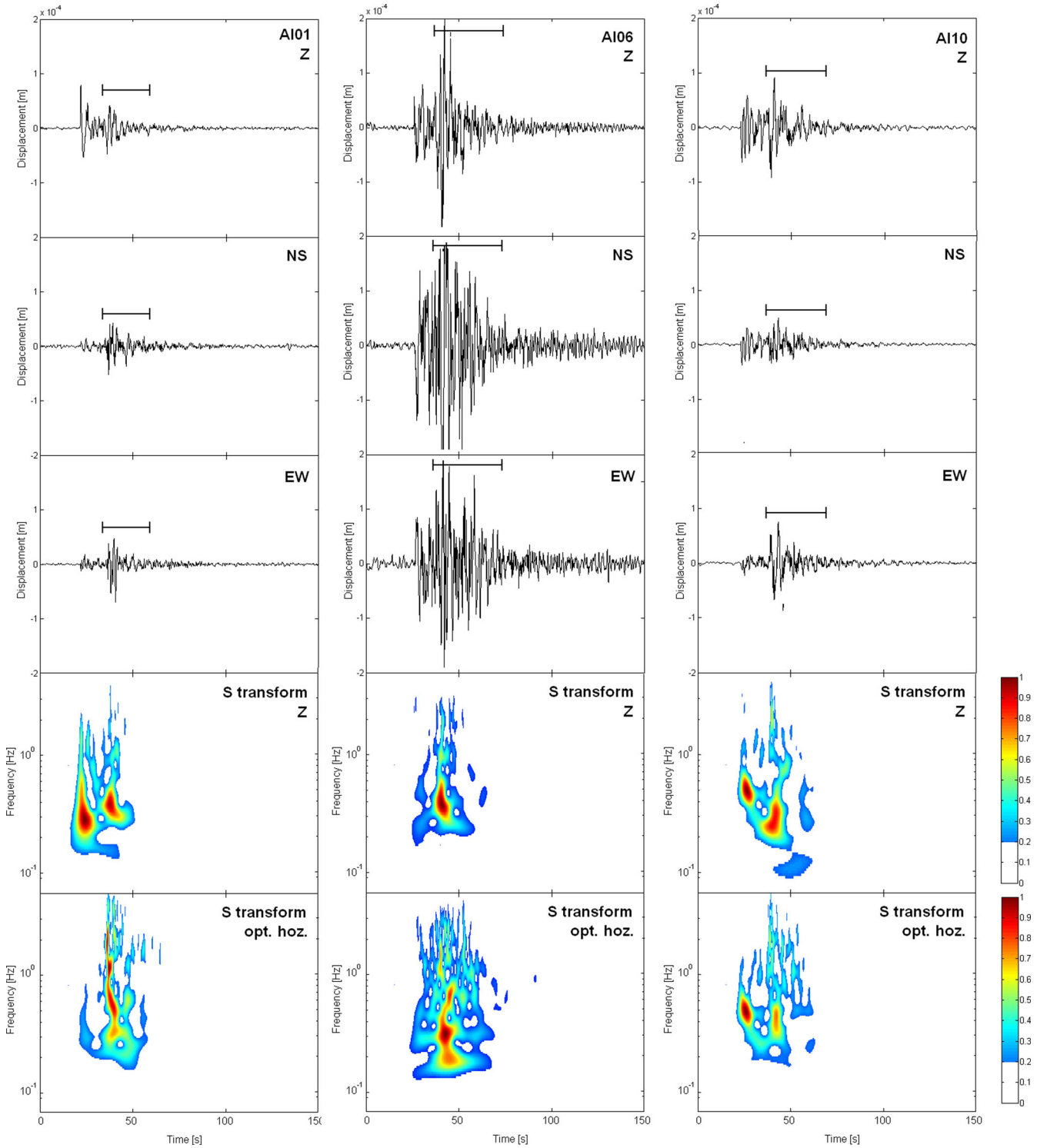

Figure 7. The displacement time series for the vertical (top row), NS (second row from top) and EW components (third row from top), normalized time–frequency analysis (*S* transform) of the vertical (second row from bottom) and of the optimized horizontal component (bottom row) for the 2014 July 30 event to the northwest of Almaty for stations Al01 (left), Al06 (middle) and Al10 (right). A threshold of 20 per cent of the maximum energy of the denoised *S* transform is applied both to the vertical and the optimized horizontal components. The time windows for *S* wave analyses (HVSR and SSR) are indicated.

parts of the city. On the other hand, for deeper layers more steady lateral velocity variations have been found. However, one cannot fully exclude this effect. For example, deviations for Al03 in Fig. 9 might have been caused by lateral heterogeneities in the central-northern part of the city as described by Kulikovsky (1973).

7 DISCUSSION

The effects of the basin edge and the thickness of the sedimentary cover on the frequency content and the amplitude of ground motion can be significant. Large mountains surrounding basins can act as a natural seismic source region by scattering and focusing waves

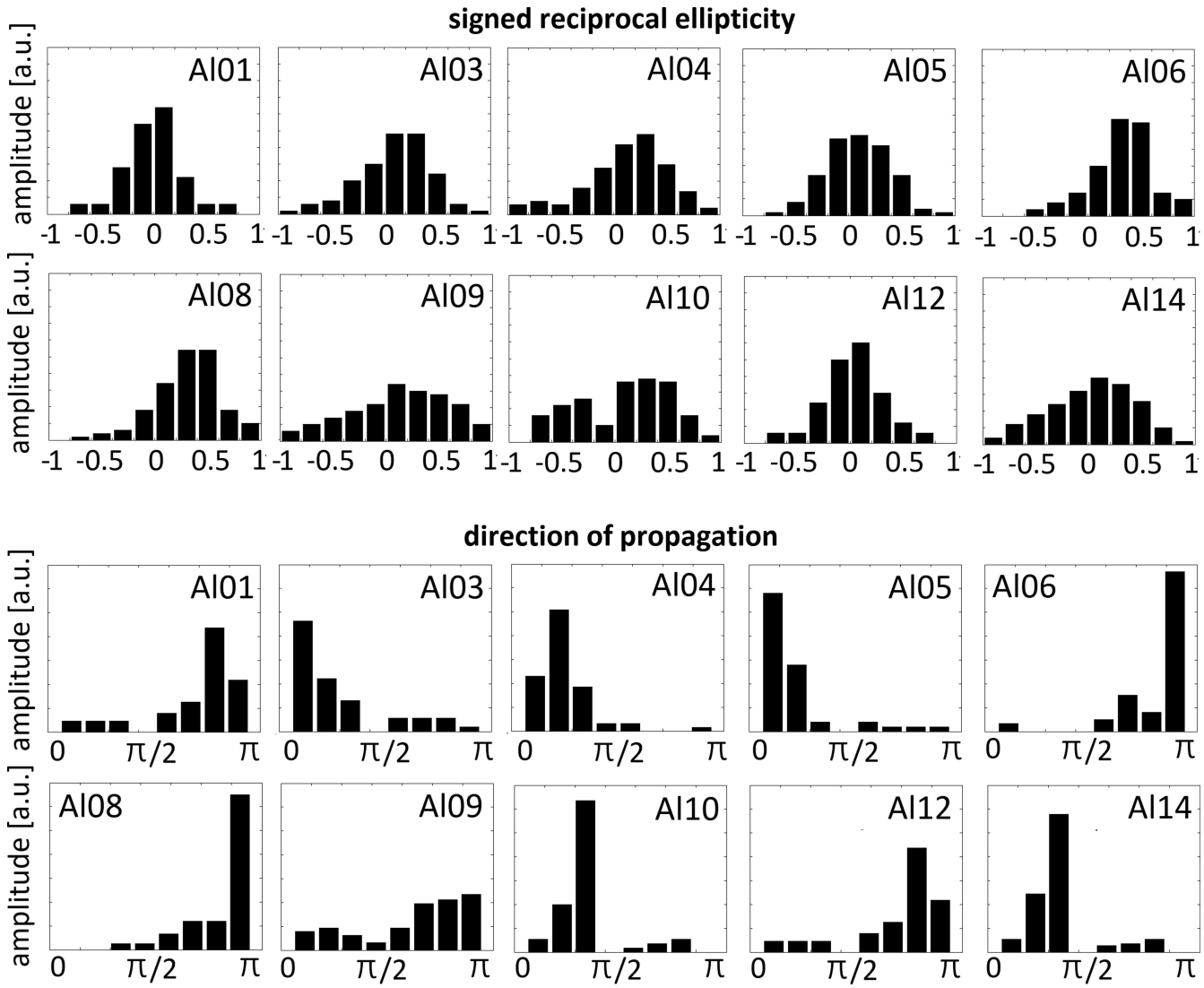

Figure 8. Normalized content of high-energy spots in the *t–f* domain for various network sites (*cf.* black ellipses in Fig. 6 for Al01, Al06 and Al10) for signed reciprocal ellipticity (top) and direction of propagation against north (bottom) for the 2014 June 13 event south of Almaty.

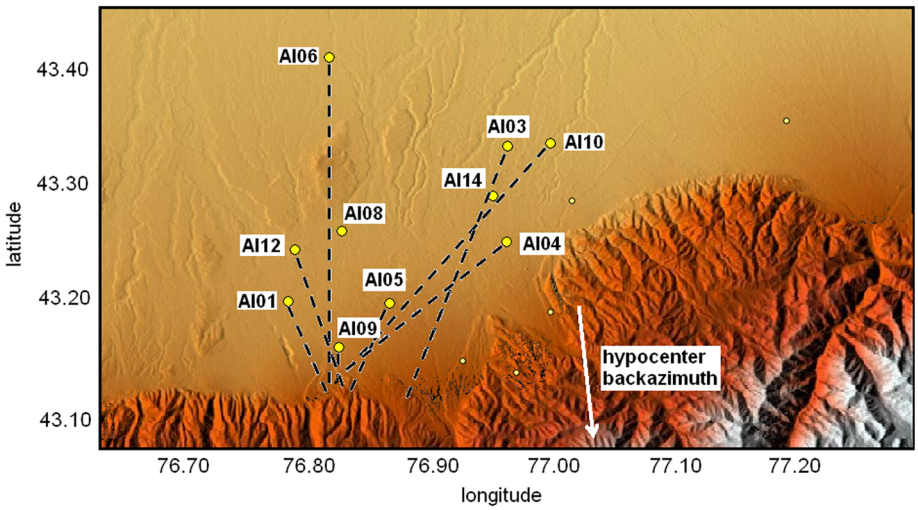

Figure 9. Possible source regions at the edge of the Almaty basin for the 2014 June 13 event. The dashed lines correspond to propagation directions for the time window of the low-frequency arrivals for network sites (yellow dots). The white arrow indicates the location of the hypocentre to the south of the Almaty basin.

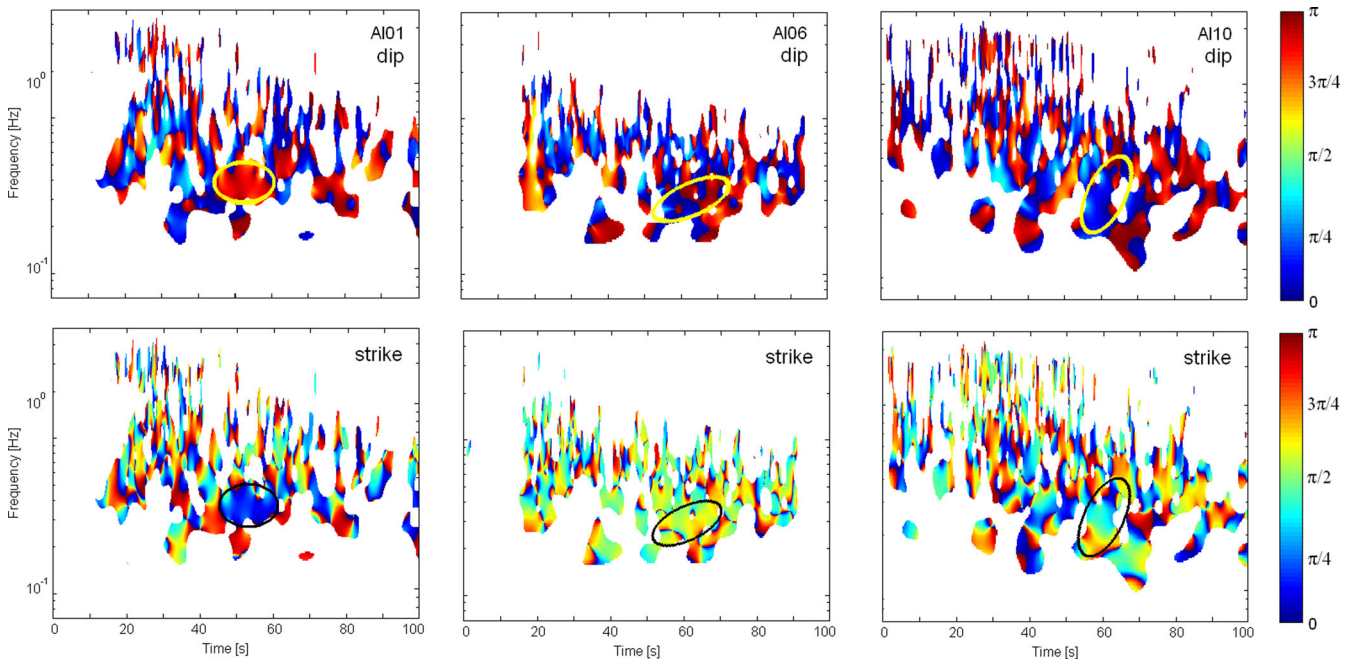

Figure 10. Inclination of the polarization ellipse I (dip, top row) and azimuth Ω (strike, bottom row) for possible basin-edge generated Rayleigh waves for event of 2014 June 13 south of Almaty at network sites Al01 (left), Al06 (middle) and Al10 (right). The ellipses mark areas of high energy.

generated by earthquakes outside the basin. *t–f* analyses (e.g. Figs 6 and 7, fourth and fifth row from top) show that for local and regional events, body waves have a relatively short duration inside the basin whereas the later part of the signal consist mainly of basin-induced surface waves which have likely been generated at the complex interface between the sedimentary cover and the bedrock outcrop at the southern edge of the Almaty basin.

As such waves can be generated at any site along the basin edge, denoising and *t–f* analyses allow a more precise identification of these waves and their direction of propagation. To this regard, we exemplarily calculate the inclination I of the polarization ellipse plane to the horizontal plane (dip, $I = \tan^{-1}[\sqrt{\vec{v}_x^2 + \vec{v}_y^2}/\vec{v}_z]$) and the azimuth Ω of the ascending node spectrum (strike, $\Omega = \tan^{-1}[\vec{v}_y/\vec{v}_x]$) for the 2014 June 13 event south of Almaty (Fig. 10). Herein, the $\vec{v}$ represent the corresponding eigenvectors of the cross-energy matrix (for all details, see Kulesh *et al*. 2007). If one follows the classical approach of Pinnegar (2006), both polarization attributes of the waves (ellipses in Fig. 10 corresponding to black ellipses in Fig. 6) would hardly allow to be identified as basin-edge generated. Following the classical approach, Rayleigh waves require $\Omega \approx 0$ which means that the particle motion is displaced in the direction of wave propagation along the direct line connecting the stations and the earthquake hypocentre (white arrow in Fig. 9). Only Al01 can fulfil this requirement: the dip and strike take values of around $3\pi/4$ and close to 0, meaning that the hypocentre direction and the direction of the secondary surface waves are almost identical. For Al06 and Al10, however, the values of the strike are clearly larger than 0, meaning that these waves cannot be identified as basin-edge induced following the classical approach. This deficiency is mainly due to the fact that for the determination of the dip and strike the waves are assumed to propagate only radial from the hypocentre and any subsequent generation sites are discarded.

For a single event, however, secondary surface waves can be generated almost all along the basin edge with very different azimuths (see the large variability of the strike values in Fig. 10 taking values between 0 and $\pi/2$). Similar observations for the generation of surface waves have already been made by Olsen (2000) and Frankel *et al*. (2001). At first glance, this might be due to the fragmented bedrock outcrop at the southern edge of the Almaty basin which leads to great complexity in the wave propagation. Although the line separating the sediment infill and the outcropping bedrock can be mapped very well, it is not only the shape along the surface but every point from the free surface to the deepest point of the basin along its wall will play a role in the generation of the surface waves (Narayan 2015). As highly resolved information on the shape of the sediment-bedrock interface is generally lacking, the generation azimuths for one single event can hardly be quantified in advance.

However, a statistical analysis on the whole dataset might allow a more quantitative assessment of the generation of secondary surface waves. To this regard, we calculated the direction of propagation for network sites Al01, Al06 and Al10 using the dataset described in Section 2. The same dataset has been used for calculating the HVSR spectral ratios. As can be seen in Fig. 11, the dependency of generation sites systematically manifests itself that most of the secondary surface waves have been generated along the south-eastern edge of the city. For Al01, around 65 per cent of the identified surface waves have been generated in the south-eastern azimuthal sector, while the percentage increases to 78 per cent for Al06. Although the thickness of sedimentary cover is not well constrained comprehensively in terms of absolute values all over the Almaty basin, for this part of the city the bedrock is known to plunge very steeply (Shatsilov 1989; see also the narrow contour lines in Fig. 11). On the contrary, much less surface waves originate from the south-western edge of the city although a large number of events did occur with this azimuth (Fig. 1). Furthermore, events from the north, as the one shown in Fig. 7, do not induce significant surface waves.

Despite the absolute amplitudes of the basin edge-generated surface waves will depend on the amplitude of the incident wave field, one can further observe that the relatively largest amplitudes

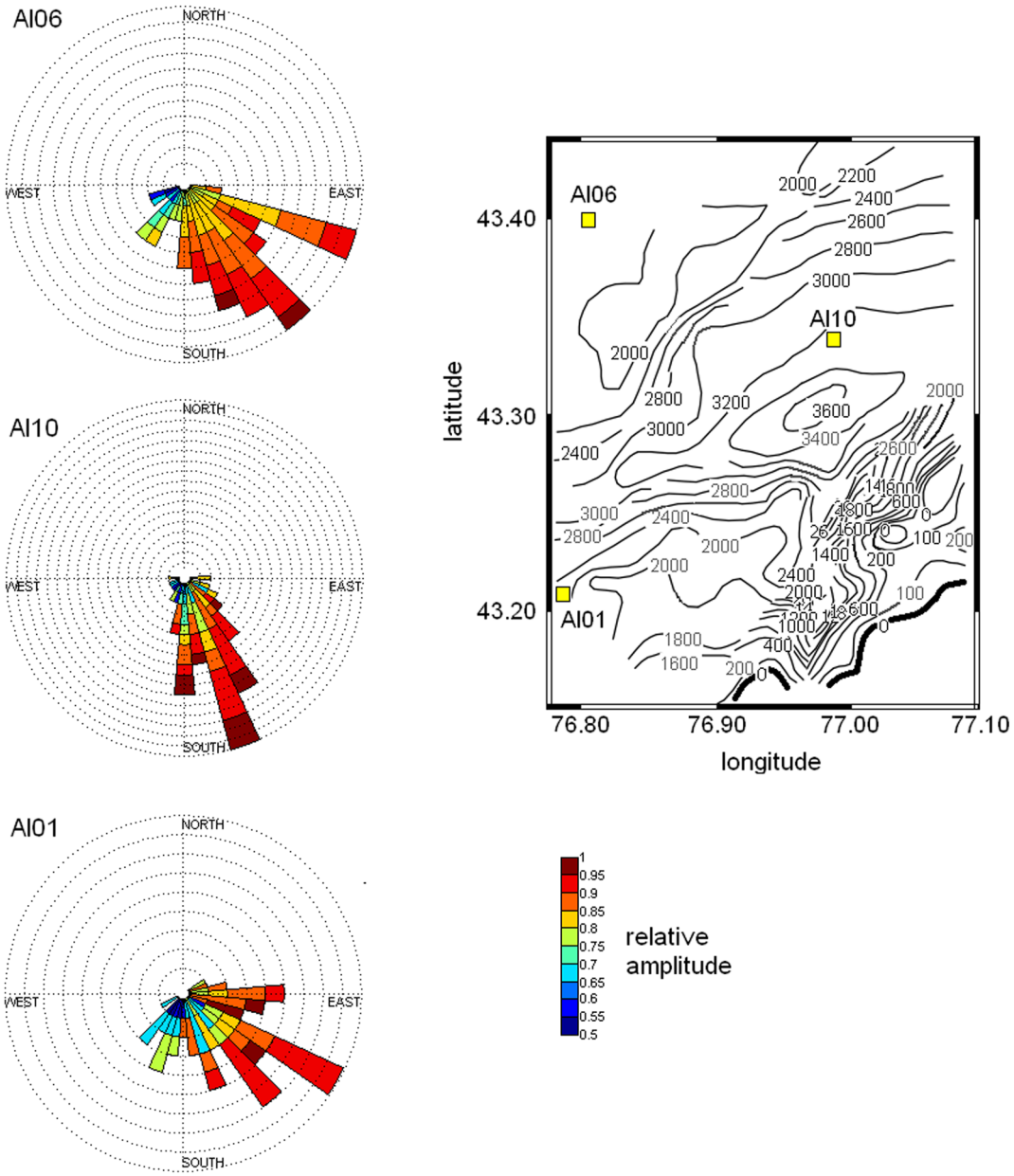

Figure 11. Direction of propagation for basin edge-induced surface waves for all events recorded at network sites Al01 (bottom left), Al06 (top left) and Al10 (middle left). The length of each bar corresponds to the number of surface waves for a given azimuth. The colour scale represents the relative amplitude of the registered surface waves. The isolines in the central plot represent the thickness of the sedimentary cover in meters below the city of Almaty (Shatsilov 1989). The basin edge is indicated by a thick black line.

(reddish colours in Fig. 11) are generated along the steepest basin edges (narrow contour lines in Fig. 11). Previous studies have found a tendency of the amplitudes of basin edge-generated surface waves to increase with soil thickness (Ji *et al*. 2000; Narayan 2005) and with angle of incidence (Bard & Bouchon 1980a), that is, shallow events will cause larger amplitudes. As can be seen in Fig. 1, although all events are rather shallow, no distinct depth pattern for the recorded events can be observed. More severe might be the influence of the shallow surface layers with *S* wave velocities as low as ∼400 m s^{-1} (Silacheva *et al*. 2014a) on the relative amplitude of the edge-generated surface waves (Miyake & Koketsu 2005). This might indicate that the largest amplitudes for waves generated at the south-eastern edge of the basin are caused by an efficient conversion due to the notably dipping shallow impedance contrast and the corresponding fast decrease of the fundamental frequency.

8 CONCLUSIONS

Multidimensional site effects have a considerable influence on earthquake ground motion in the Almaty basin. This observation is consistent with the relatively large damages which have been observed in the city already during previous events like the 1889 Chilik earthquake. The comparison between the HVSR and SSR results illustrates a generally good agreement in the shape of all curves, especially for the moderate peak of the fundamental resonance frequency around 0.2 Hz. An extension of the classical

spectral ratio method, the mean group delay technique, allows the phase modifications between a reference site and on the site under study to be obtained. Although the group delay is inherently linked to the (frequency-dependent) signal duration, there are significant site-specific modifications in phase and changes in signal duration at frequencies higher than the fundamental one. Combining a time-frequency analysis (*S* transform) and polarization properties of the seismic waves, we verified the influence of locally generated Rayleigh waves and converted phases contributing to amplification effects at low frequencies between 0.15 and 0.4 Hz. The computed polarization attributes can be directly associated with the azimuthal direction of wave propagation irrespectively of the hypocentre location. The method can help in identifying secondary waves even when the direction of propagation does not coincide with the hypocentre direction. Although the identification and characterization of individual waves packages for a single event might be rather uncertain due to the complex basin shape, a preferential range for the generation of secondary surface waves along the south-eastern edge of the basin could be identified, coinciding with the steepest slope of the bedrock around the Almaty basin. Therefore, the combined application of the presented methods might contribute both for an improved understanding of the wave field at sites at which the spatial variability of ground motion is not only related to a simple 1-D response. This might allow developing more sophisticated methods accounting for secondary surface waves as well as taking these waves into account for better constrained assessment of the level of seismic hazard.

ACKNOWLEDGEMENTS

We are very grateful for the collaboration and support given to us during the survey measurements and the data collection by many people in Almaty. We thank people from Institute of Seismology of the Republic of Kazakhstan for the help during the field work. Kevin Fleming kindly revised our English. The detailed comments and suggestions of two anonymous reviewers and editor Martin Schimmel greatly improved the manuscript. Instruments were provided by the Geophysical Instrumental Pool Potsdam (GIPP). This research has been supported by the Global Change Observatory Central Asia of the GFZ and the Earthquake Model Central Asia (EMCA).

REFERENCES

Abdrakhmatov, K.E., Djanuzakov, K.D. & Delvaux, D., 2002. Active tectonics and seismic hazard of the Issyk-Kul Basin in the Kyrgyz Tian-Shan, in *Lake Issyk-Kul: Its Natural Environment*, Vol. 13, eds Klerx, J. & Imanackunov, B., Springer Science & Business Media.

Aki, K. & Larner, K.L., 1970. Surface motion of a layered medium having an irregular interface due to incident plane *SH* waves, *Earth Planets Space*, **75,** 399–405.

Alterman, Z. & Karal, F.C., 1968. Propagation of elastic waves in layered media by finite difference methods, *Bull. seism. Soc. Am.*, **58,** 367–398.

Anderson, J.G., Bodin, P., Brune, J.N., Prince, J., Singh, S.K., Quaas, R. & Ofiate, M., 1986. Strong ground motion from the Michoacan Mexico earthquake, *Science*, **233,** 1043–1049.

Bard, P.Y., 1995. Effects of surface geology on ground motion: recent results and remaining issues, in *10th European Conference on Earthquake Engineering*, pp 305–323, ed. Duma, G., A. A. Balkema Publishers.

Bard, P.Y., 1999. Microtremor measurements: a tool for site effect estimation, in *The Effects of Surface Geology on Seismic Motion*, Vol. 3, pp. 1251–1279, Balkerna, Rotterdam.

Bard, P.Y. & Bouchon, M., 1980a. The seismic response of sediment-filled valleys. Part 1. The case of incident *SH* waves, *Bull. seism. Soc. Am.*, **70,** 1263–1286.

Bard, P.Y. & Bouchon, M., 1980b. The seismic response of sediment-filled valleys. Part 2. The case of incident *P* and *SV* waves, *Bull. seism. Soc. Am.*, **70,** 1921–1941.

Beauval, C., Bard, P.Y., Moczo, P. & Kristek, J., 2003. Quantification of frequency-dependent lengthening of seismic ground-motion duration due to local geology: applications to the Volvi area (Greece), *Bull. seism. Soc. Am.*, **93,** 371–385.

Bindi, D., Parolai, S., Gómez-Capera, A., Locati, M., Kalmetyeva, Z. & Mikhailova, N., 2014. Locations and magnitudes of earthquakes in Central Asia from seismic intensity data, *J. Seismol.*, **18,** 1–21.

Bogdanovich, K.I., 1911. An earthquake of December 22, 1910 (January 4, 1911) in northern chains of the Tien Shan between Verny and Issyk-Kul, *Proceedings of Geological Committee*, **30,** 329–419 (in Russian).

Bogdanovich, M.M.C., Kark, J., Korolkov, B. & Muchketov, D., 1914. Earthquake of the 4th January 1911 in the northern districts of the Tien Shan, *Tr. Geol. Com. Ser*, **89,** 101–108.

Boore, D.M. & Bommer, J.J., 2005. Processing of strong-motion accelerograms: needs, options and consequences, *Soil Dyn. Earthq. Eng.*, **25,** 93–115.

Boore, D.M., Lamer, K. & Aki, K., 1971. Comparison of two independent method for the solution of wave scattering problems: Response of sedimentary basin to vertically incident *SH* waves, *J. geophys. Res.*, **76,** 558–569.

Borcherdt, R.D., 1970. Effects of local geology on ground motion near San Francisco Bay, *Bull. seism. Soc. Am.*, **60,** 29–61.

Chedia, O.K., Abdrakhmatov, K.E., Korzhenkov, A.M. & Lemzin, I.N., 1998. Seismotectonic position of the Balasogun, north Tien Shan earthquake of the 15th century, *J. Earthq. Predict. Res.*, **7,** 289–299.

Cornou, C., Bard, P.Y. & Dietrich, M., 2003. Contribution of dense array analysis to the identification and quantification of basin-edge-induced waves, Part II: Application to Grenoble basin (French Alps). *Bull. seism. Soc. Am.*, **93,** 2624–2648.

Davis, P.M., Rubinstein, J.L., Liu, K.H., Gao, S.S. & Knopoff, L., 2000. Northridge earthquake damage caused by geologic focusing of seismic waves, *Science*, **289,** 1746–1750.

Duval, A.M., 1996. Determination de la response d'un site aux seismes a aide du bruit de fond: Evaluation expermentale, *PhD thesis*, 265 pages, Paris, France (in French).

Frankel, A., Hough, S., Friberg, P. & Busby, R., 1991. Observations of Loma Prieta aftershocks from a dense array in Sunnyvale, California, *Bull. seism. Soc. Am.*, **81,** 1900–1922.

Frankel, A., Carver, D., Cranswick, E., Bice, T., Sell, R. & Hanson, S., 2001. Observations of basin ground motions from a dense seismic array in San Jose, California, *Bull. seism. Soc. Am.*, **91,** 1–12.

Furumura, T. & Hayakawa, T., 2007. Anomalous propagation of long-period ground motions recorded in Tokyo during the 23 October 2004 M_w 6.6 Niigata-ken Chuetsu, Japan, Earthquake, *Bull. seism. Soc. Am.*, **97,** 863–880.

Gabor, D., 1946. Theory of communication. Part 1: the analysis of information, *J. Inst. Electr. Eng.*, **93,** 429–441.

Galiana-Merino, J.J., Rosa-Herranz, J.L. & Parolai, S., 2008. Seismic P phase picking using a Kurtois-based criterion in the stationary wavelet domain, *IEEE Trans. Geosci. Remote Sens.*, **46,** 3815–3826.

Gao, S., Liu, H., Davis, P.M. & Knopoff, L., 1996. Localized amplification of seismic waves and correlation with damage due to Northridge earthquake, *Bull. seism. Soc. Am.*, **86,** 209–230.

Hallier, S., Chaljub, E., Bouchon, M. & Sekiguchi, H., 2008. Revisiting the basin-edge effect at Kobe during the 1995 Hyogo-Ken Nanbu earthquake, *Pure appl. Geophys.*, **165,** 1751–1760.

Hanks, T.C., 1975. Strong ground motion of the San Fernando, California, earthquake: Ground displacements, *Bull. seism. Soc. Am.*, **65,** 193–225.

Hong, T.L. & Helmberger, D.V., 1978. Glorified optics and wave propagation in non planar structures, *Bull. seism. Soc. Am.*, **68,** 1313–1330.

Horike, M., Uebayashi, H. & Takeuchi, Y., 1990. Seismic response in three-dimensional sedimentary basin due to plane *S* wave incidence, *J. Phys. Earth*, **38,** 261–284.

Huang, B.S., Huang, Y.L., Lee, S.J., Chen, C.H., Chen, K.C., Huang, W.G. & Tsao, S., 2010. Array Observations for Long-Period Basin Ground Motions in the Taipei Region during the M 7.1 Eastern Taiwan Offshore Earthquake of 31 March 2002, *Terr. Atmos. Ocean. Sci.*, **21,** 477–484.

Ignatiev, I.V., 1886. Earthquake in the Tokmak district in 1885, *Proc. of the Imperial Russian Geographic Society*, **22,** 150–164.

Japan International Cooperation Agency, 2009, The study on earthquake disaster risk management for Almaty city in the Republic of Kazakhstan: Final report, in *Evaluation of Earthquake Hazards and Risks in Almaty City*, Vol. 2, pp. 281, Japan International Cooperation Agency.

Ji, C., Helmberger, D.V. & Wald, D.J., 2000. Basin structure estimation by waveform modeling: forward and inverse methods, *Bull. seism. Soc. Am.*, **90,** 964–976.

Kawase, H., 1987. Irregular ground analysis to interpret time-characteristics of strong motion recorded in Mexico City during 1985 Mexico earthquake, in *Ground Motion and Engineering Seismology, Development in Geotechnical Engineering*, Vol. 44, pp. 467–476, ed. Cakmak, A.S., Elsevier Scientific Publishing.

Kawase, H., 1996. The cause of the damage belt in Kobe: The basin-edge effect, constructive interference of the direct *S*-wave with the basin-induced diffracted/Rayleigh waves, *Seismol. Res. Lett.*, **67,** 25–34.

Koketsu, K. & Kikuchi, M., 2000. Propagation of seismic ground motion in the Kanto basin, Japan, *Science*, **288,** 1237–1239.

Konno, K. & Ohmachi, T., 1998. Ground-motion characteristics estimated from spectral ratio between horizontal and vertical components of microtremor, *Bull. seism. Soc. Am.*, **88,** 228–241.

Korjenkov, A., Baipakov, K., Chang, C., Peshkov, Y. & Savelieva, T., 2004. Traces of ancient earthquakes in medieval cities along the Silk Road, northern Tien Shan and Dzhungaria, *Turk. J. Earth Sci.*, **12,** 241–261.

Kulesh, M., Diallo, M.S., Holschneider, M., Kurennaya, K., Krüger, F., Ohrnberger, M. & Scherbaum, F., 2007. Polarization analysis in the wavelet domain based on the adaptive covariance method, *Geophys. J. Int.*, **170,** 667–678.

Kulikovsky, K.T., 1973. Geological map of the city of Almaty, 1:25000, *Novosti Nauki Kazakhstana* 1, Alma-Ata, Kazakh SSR.

Kyurskeyev, A., Nurmagambetov, A., Sydykov, A., Mikhailova, N. & Shatsilov, V.I., 1993. Detailed Seismic Zoning of Almaty Industrial Area, *Novosti Nauki Kazakhstana* 1, Alma-Ata, Kazakhstan.

Lermo, J. & Chávez-García, F.J., 1993. Site effect evaluation using spectral ratios with only one station, *Bull. seism. Soc. Am.*, **83,** 1574–1594.

Liu, H.L. & Heaton, T., 1984. Array analysis of the ground velocities and accelerations from the 1971 San Fernando, California, earthquake, *Bull. seism. Soc. Am.*, **74,** 1951–1968.

Maufroy, E. *et al.*, 2017. Source-related variability of site response in the Mygdonian Basin (Greece) from accelerometric recordings and 3D numerical simulations, *Bull. seism. Soc. Am.*, **107,** 787–808.

McGuire, R.K., 2004. Seismic hazard and risk analysis, EERI monograph MNO-10. Earthquake Engineering Research Institute, Oakland, California.

Meza-Fajardo, K.C., Papageorgiou, A.S. & Semblat, J.F., 2015. Identification and extraction of surface waves from three-component seismograms based on the normalized inner product, *Bull. seism. Soc. Am.*, **105,** 210–229.

Mikhailova, N., 1996. Seismic hazard in quantity characteristics of strong ground motions (on the example of Almaty). *PhD thesis*, University of Almaty, Kazakhstan.

Miyake, H. & Koketsu, K., 2005. Long-period ground motions from a large offshore earthquake: the case of the 2004 off the Kii peninsula earthquake, Japan, *Earth Planets Space*, **57,** 203–207.

Morozov, I.B. & Smithson, S.B., 1996. Instantaneous polarization attributes and directional filtering, *Geophys.*, **61,** 872–881.

Mushketov, I.V., 1888. The earthquake of 28 May 1887 in the city Verny, *Izv. Imp. Russ. Geogr. Surv.*, **14,** 65.

Mushketov, I.V., 1899. *Physical Geology*, Ehrlich.

Mushketov, I.V. & Orlov, A.P., 1893. Catalogue of earthquakes of Russian Empire, *Notes of Russian Geographic Soc.*, pp. 582, St. Peterburg (in Russian).

Mushketov, I.V. & Survorin, A.S., 1891. *Materials for the Study of Earthquakes of Russia*, *Commission of the Geology Committee*.

Narayan, J.P., 2005. Study of basin-edge effects on the ground motion characteristics using 2.5-D modeling, *Pure appl. Geophys.*, **162,** 273–289.

Narayan, J.P., 2012. Effects of *P*-wave and *S*-wave impedance contrast on the characteristics of basin transduced Rayleigh waves, *Pure appl. Geophys.*, **169,** 693–709.

Narayan, J.P., 2015. 3D basin-shape ratio effects on frequency content and spectral amplitudes of basin-generated surface waves and associated spatial ground motion amplification and differential ground motion, *J. Seimsol.*, **19,** 293–316.

Nurmagambetov, A., 1999. *Seismic History of Almaty*, p 67, ed. Khalturin, V.I., LEM.

Nurmagambetov, A., Mikhailova, N. & Iwan, W., 1999. Seismic hazard of the Central Asia region, in *Seismic Hazard and Building Vulnerability in Post-Soviet Central Asian Republics*, pp. 1–43, Springer.

Olsen, K.B., 2000. Site amplification in the Los Angeles basin from three-dimensional modeling of ground motion, *Bull. seism. Soc. Am.*, **90,** 77–94.

Papoulis, A., 1962. *Fourier Transform and Its Applications*, McGraw-Hill.

Parolai, S., 2009. Denoising of seismograms using the S transform, *Bull. seism. Soc. Am.*, **99,** 226–234.

Petrovic, B., Pilz, M. & Parolai, S., 2018. Identification of basin-edge generated Rayleigh waves by using the *S* transform and polarization attributes, *Geophys. J. Int*., submitted.

Pilz, M. & Parolai, S., 2016. Ground-motion forecasting using a reference station and complex site-response functions accounting for the shallow geology, *Bull. seism. Soc. Am.*, **106,** 1570–1583.

Pinnegar, C.R., 2006. Polarization analysis and polarization filtering of three-component signals with the time-frequency *S* transform, *Geophys. J. Int.*, **165,** 596–606.

Rau, J.L., 2003. Almaty, Kazakhstan, in *The ground beneath our feet: A factor in urban planning, Economic and Social Commission for Asia and the Pacific*, pp. 488, ed. Bernholz, C.D., United Nations Publications.

Rene, R.M., Fitter, J.L., Forsyth, P.M., Kim, K.Y., Murray, D.J., Walters, J.K. & Westerman, J.D., 1986. Multicomponent seismic studies using complex trace analysis, *Geophysics*, **51,** 1235–1251.

Roten, D., Olsen, K.B., Pechmann, J.C., Cruz-Atienza, V.M. & Magistrale, H., 2011. 3D simulations of M 7 earthquakes on the Wasatch fault, Utah, Part I: Long-period (0–1 Hz) ground motion, *Bull. seism. Soc. Am.*, **101,** 2045–2063.

Rovelli, A., Scognamiglio, L., Marra, F. & Caserta, A., 2001. Edge-diffracted 1-sec surface waves observed in a small-size intramountain basin (Colfiorito, central Italy), *Bull. seism. Soc. Am.*, **91,** 1851–1866.

Sawada, S., 1998. Phase characteristics on site amplification of layered ground with irregular interface, in *The Effects of Surface Geology on Seismic Motion*, pp. 1009–1013, eds Irikura, K., Kudo, K., Okada, H. & Sasatani, T., Balkema.

Semblat, J.F., Kham, M., Parara, E., Bard, P.Y., Pitilakis, K., Makra, K. & Raptakis, D., 2005. Seismic wave amplification: Basin geometry vs soil layering, *Soil Dyn. Earthq. Eng.*, **25,** 529–538.

Shatsilov, V.I., 1989, Survey technique for seismic hazard assessment, Nauka, Alma-Ata, Kazakh SSR, pp. 208. (in Russian).

Silacheva, N., Kulbayeva, U. & Kravchenko, N., 2014a. Seismic ground motion variations resulting from site conditions, *Geod. Geodyn.*, **5,** 9–15.

Silacheva, N., Kulbayeva, U. & Kravchenko, N., 2014b. Catalogs of ground-motion parameters for earthquake prone regions in Kazakhstan, *Geod. Geodyn.*, **5,** 20–26.

Smith, B.D. & Ward, S.H., 1974. On the computation of polarization ellipse parameters. *Geophysics*, **39,** 867–869.

SNIP, 2001. 2.07-03-2001, Building standards and buildings in Almaty and in the surrounding areas, taking into account the seismic microzonation, Gosstry, Moscow (in Russian).

Stephenson, W.R., 2003. Factors bounding prograde Rayleigh-wave particle motion in a soft-soil layer, *Proc. 2003 Pacific Conference on Earthquake Engineering*, Christchurch, New Zealand.

Stockwell, R.G., Mansinha, L. & Lowe, R.P., 1996. Localization of the complex spectrum: the *S* transform, *IEEE Trans. Signal Process.*, **44,** 998–1001.

Takemura, S., Akatsu, M., Masuda, K., Kajikawa, K. & Yoshimoto, K., 2015. Long-period ground motions in a laterally inhomogeneous large sedimentary basin: observations and model simulations of long-period surface waves in the northern Kanto Basin, Japan, *Earth Planets Space*, **67,** 33.

Tanimoto, T. & Rivera, L., 2005. Prograde Rayleigh wave particle motion, *Geophys. J. Int.*, **162,** 399–405.

Toriumi, I., 1975. Earthquake characteristics in plain, in *Proceedings of 4th Japan Earthquake Engineering Symposium*, pp 129–136, Tokyo (in Japanese).

Trifonov, V.G., Soboleva, O.V., Trifonov, R.V. & Vostrikov, G.A., 2002. Recent geodynamics of the Alpine-Himalayan collision belt, *Transactions of the Geological Institute RAS*, Vol. 541, pp. 224, GEOS, Moscow (in Russian).

Trifunac, M.D., 1971. Surface motion of a semi-cylindrical alluvial valley for incident plane *SH* waves, *Bull. seism. Soc. Am.*, **61,** 1755–1770.

Ulomov, V.I., Polyakova, T.P. & Medvedeva, N.S., 2002. On the long-term prediction of strong earthquakes in central asia and the black sea-caspian region, *Izv. Phys. Sol. Earth*, **38,** 276–290.

Velitzky, S.N., 1911. An earthquake in Verny town and Semirechie Oblast (Region) of December 22, 1910 and January 4, 1911, *Proc. Emperor Russian Geographical Society*, I/IV, 113–163 (in Russian).

Vershinin, P., 1889. An earthquake in Verny town of Semirechie Oblast (Region), *Notes of Western Siberian Division of Emperor Russian Geographical Society*, **10,** 1–23 (in Russian).

Vidale, J.E., 1986. Complex polarization analysis of particle motion, *Bull. seism. Soc. Am.*, **76,** 1393–1405.

Vidale, J.E. & Helmberger, D.V., 1988. Elastic finite-difference modeling of the 1971 San Fernando, California earthquake, *Bull. seism. Soc. Am.*, **78,** 122–141.

Yoshimoto, K. & Takemura, S., 2014. A study on the predominant period of long-period ground motions in the Kanto Basin, Japan, *Earth Planets Space*, **66,** 100, doi:10.1186/1880-5981-66-100.